LEAKAGE AND ROTORDYNAMIC EFFECTS OF COMPRESSIBLE ANNULAR SEALS

by

Joseph K. Scharrer

President

and

Joseph M. Pelletti

General Manager

Rotordynamics-Seal Research

North Highlands, California

Joseph K. Scharrer is President and Founding Partner of Rotordynamic-Seal Research and has over 12 years of experience in turbomachinery design, analysis and testing. He has authored or coauthored over 45 technical papers dealing with the design, analysis, and testing of seals and fluid film bearings for rotordynamics. Dr. Scharrer's employment includes Dresser Atlas Oilfield Services Group, General Electric Aircraft Engine Group, and Rocketdyne Division of Rockwell International. He holds four patents and has three patents pending for hydrostatic bearing, seals, and magnetic bearings and has been awarded numerous NASA technology utilization awards. Dr. Scharrer's education includes a B.S. degree (Engineering) from Northern Arizona University (1982), an M.S. degree (Mechanical Engineering) (1985), and a Ph.D. (Mechanical Engineering) (1987) both from Texas A&M University.

Joseph M. Pelletti is currently General Manager of Rotordynamics-Seal Research with responsibility for all commercial engineering projects. He has authored or coauthored four technical papers dealing with the design, analysis, and testing of annular seals. Mr. Pelletti's employment includes KMC Bearing, Pratt & Whitney Aircraft, Emhart Hardware, and Sverdrup Technology. His education includes a B.S.M.E. from Northwestern University (1988) and an M.S.M.E. from Texas A&M University (1990).

INTRODUCTION

Technology for fluid handling machinery such as compressors and turbines is being pushed more and more toward higher efficiency, higher power density, and lower emissions. Achieving these performance objectives will require a complete system design approach focused on minimizing both internal and external losses. A key system component that directly controls internal and external losses is the annular seal. The strong influence of seals on turbomachinery efficiency is illustrated in Figure 1. The figure shows turbine efficiency as a function of tip clearance ratio. The results indicate that use of a shrouded rotor (that has annular seals) can substantially improve efficiency.

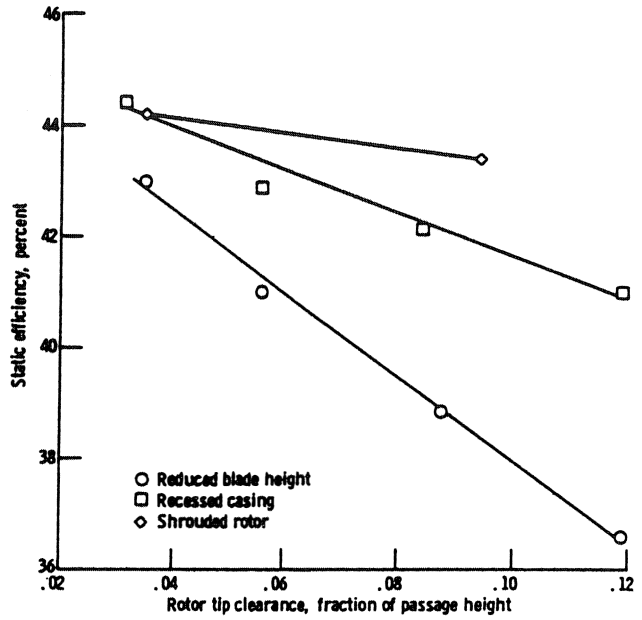

Figure 1. Effect of Tip Clearance on Turbine Efficiency.

Annular seals have been in use since modern turbomachinery came into existence. During the last 100 years, there has been a substantial amount of effort expended worldwide to investigate the characteristics of annular seals and to develop new technologies to improve their performance. Many configurations of annular seals have been developed and tested. The variety of designs is endless. Regardless of the configuration, most seals can be categorized according to the function served in the system. Typical seal categories are:

- Impeller eye seal
- Interstage seal
- Balance piston seal
- Tip seal
- Buffer seal

A typical centrifugal impeller configuration is illustrated in Figure 2 with an impeller eye and interstage seal. The purpose of the impeller eye seal is to prevent the flow of fluid from the high pressure discharge of the impeller back to the low pressure inlet. Similarly, the interstage seal prevents the flow of fluid from a high pressure cavity between the crossover and impeller eye

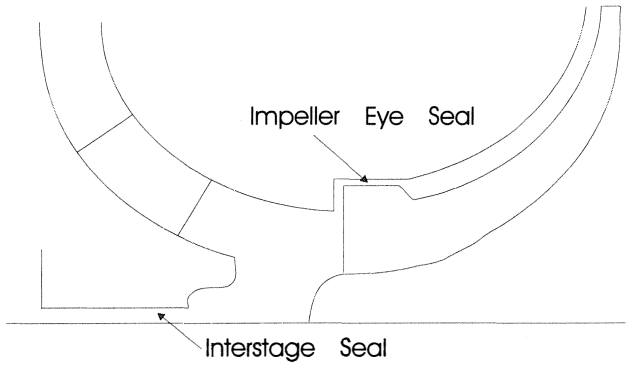

Figure 2. Example of Impeller Eye and Interstage Seal.

back to a lower pressure cavity at the back face of the previous impeller.

A typical centrifugal impeller configuration with a balance piston seal is shown in Figure 3. The balance piston seal is used to provide leakage control between a high pressure cavity and a lower pressure cavity. In addition, the balance piston seal (as its name implies) is used to control axial thrust.

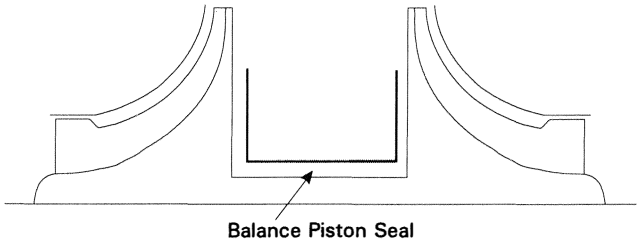

Figure 3. Example Balance Piston Seal.

A typical axial flow configuration with an interstage seal is depicted in Figure 4. Like the interstage seal configuration in the centrifugal flow machine, this seal prevents the flow of fluid from a high pressure stage to a lower pressure stage.

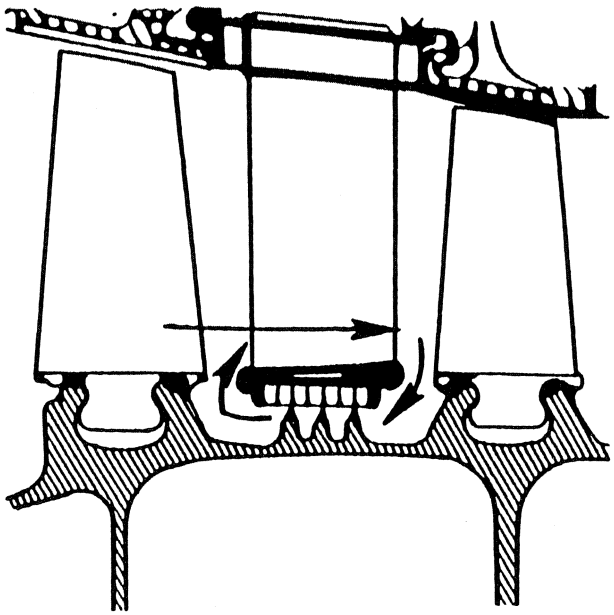

Figure 4. Example Interstage Seal for Axial Flow Machines.

BASIC SEAL CONFIGURATIONS

The number of different configurations of annular seals is only limited by the imagination. Presented here is a brief overview of the basic configurations of annular seals. First labyrinth seals are reviewed followed by bushing seals.

Labyrinth Seals

Labyrinth seals were one of the first seal configurations used in modern turbomachinery and are by far the most widely used clearance seal configuration today. The classic see-through labyrinth seal configuration is shown in Figure 5. The configuration shown is the teeth-on-stator. The same basic configuration holds when the teeth are on the rotor and the stator is smooth. Machined labyrinth teeth typically have an included angle of 12 to 15 degrees. In many cases, constant thickness strips (J-strips) of material are inserted into the housing to form the teeth. See-through labyrinth seals are used extensively in both compressors and turbines. Typically teeth-on-stator seals are used for the former and teeth-on-rotor seals are used for the latter.

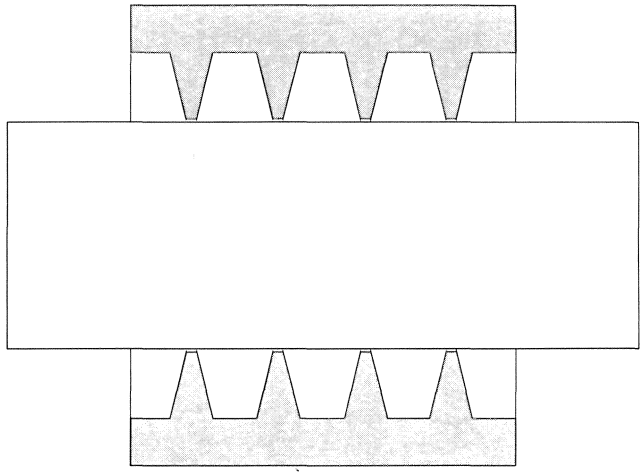

Figure 5. Example of See-through Labyrinth Seal.

A variation is shown in Figure 6 of the see-through seal; the angled tooth seal. This seal configuration has teeth that are angled into the oncoming flow. The optimum angle of the teeth

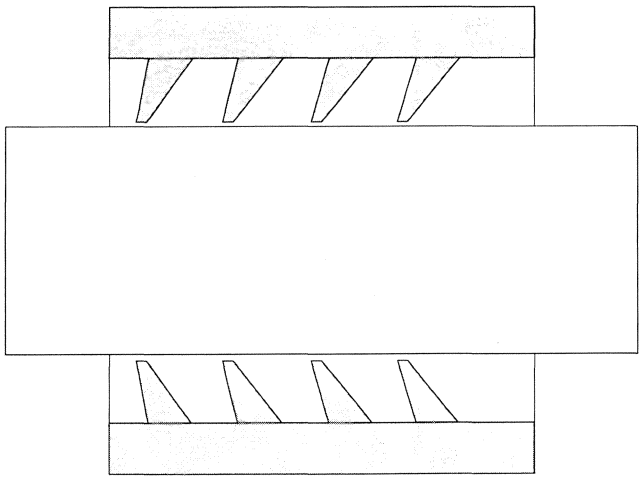

Figure 6. Example of Angled Tooth Labyrinth Seal.

is in the range of 40 to 50 degrees from vertical. This configuration is used in gas turbines and in many polymer seal applications.

A staggered labyrinth seal configuration is presented in Figure 7. The staggered labyrinth seal has a rotor that steps up and down and teeth on the stator that may or may not be the same length. In many cases, the teeth are made using J-strips. When using a staggered configuration, care must be taken to limit axial shaft travel. This configuration is used extensively in steam turbines and compressors.

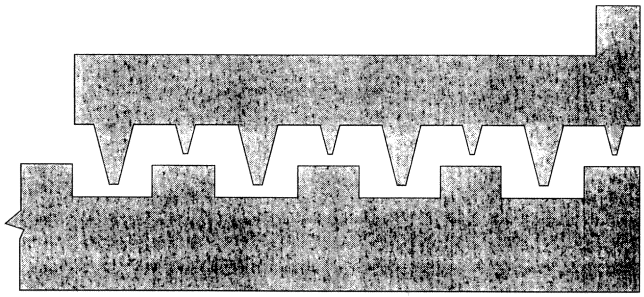

Figure 7. Example of Staggered Labyrinth Seal.

A stepped labyrinth seal configuration is portrayed in Figure 8. The rotor can step up or down depending on the flowpath requirements. The stepped seal can also be configured with angled teeth. As with the staggered seal, great care must be taken to limit axial travel when using this seal configuration. This configuration is used extensively in buffer seals, eye seals, and for seals on the back side of impellers.

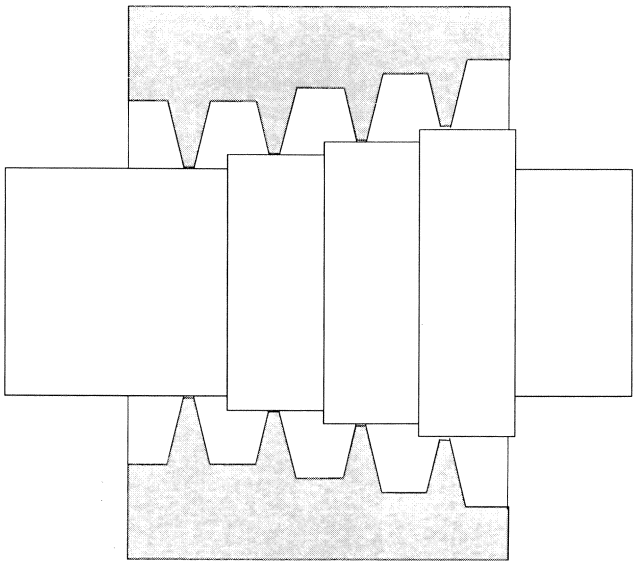

Figure 8. Example of a Stepped Labyrinth Seal.

An interlocking labyrinth seal configuration is shown in Figure 9. In this case, there are teeth on the rotor and stator. The stator is a half shell that is fitted about the shaft at assembly. As with staggered and stepped seals, great care must be taken to limit axial shaft travel when using this seal. This configuration has been used extensively in the past, however, high cost and design difficulties have caused interest to wane.

For teeth-on-rotor labyrinth seals, there are also many options with respect to stator materials and configurations. Many turbomachines employ abradable materials, such as felt metal or honeycomb, which allow the teeth to cut in during high speed operation, as illustrated in Figure 10. This results in a substantially smaller effective clearance and reduced leakage. Abradable stator materials are used extensively in gas turbine applications.

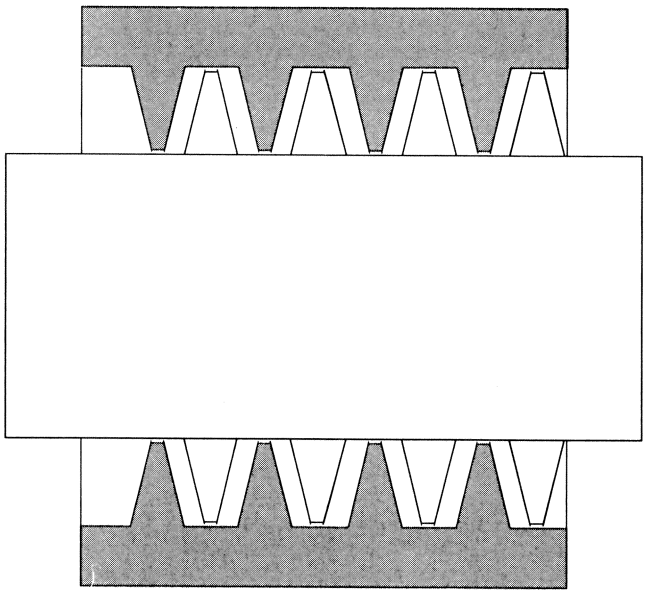

Figure 9. Example of an Interlocking Labyrinth Seal.

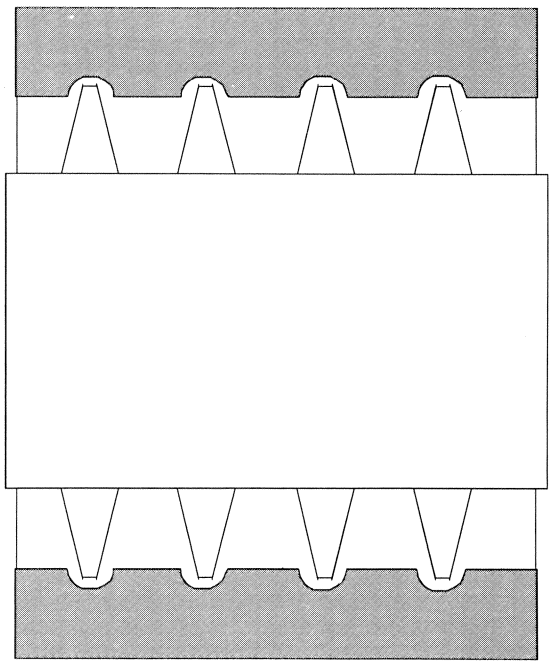

Figure 10. Example of an Abradable Labyrinth Seal.

Bushing Seals

Historically, bushing seals have not been used in primary sealing applications such as eye seals, interstage seals, and balance piston seals due to inferior leakage performance compared to labyrinth seals and concerns about rubbing. Their

application was mainly restricted to floating ring seals. Recently, bushing seals have been appearing more and more in high pressure sealing applications in the form of honeycomb stators and smooth rotors. The reason for this resurgence will become apparent by the end of this discussion.

As the name bushing seal suggests, the most common configuration is a plain cylindrical bore and smooth rotor as illustrated in Figure 11.

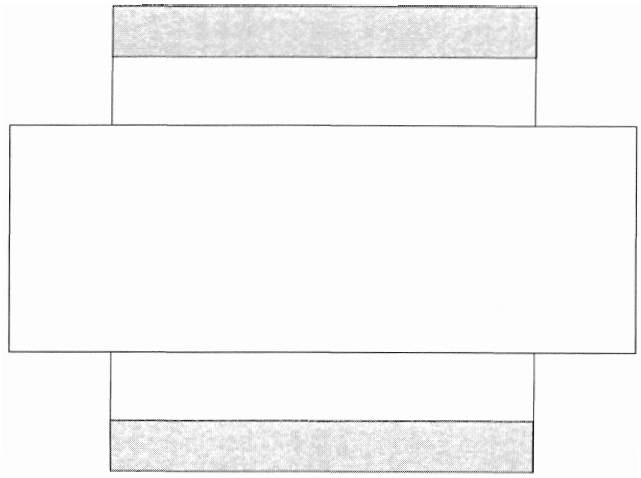

Figure 11. Example of Plain Cylindrical Bushing Seal.

A seal with a tapered bore and a smooth rotor is depicted in Figure 12. This configuration is very popular for floating ring seals due to its self centering ability and wear characteristics.

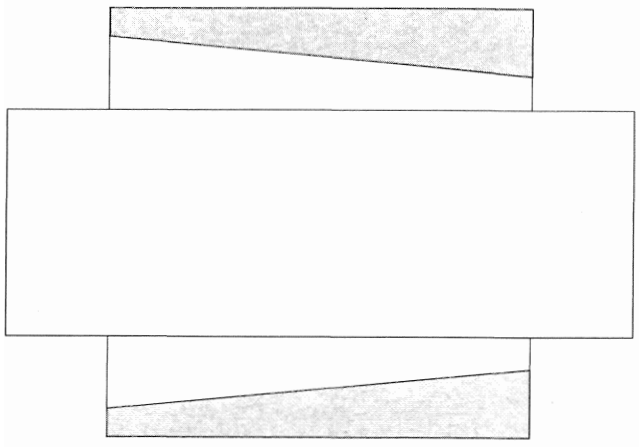

Figure 12. Example of Tapered Bore Bushing Seal.

A seal with a stepped bore and a smooth rotor is shown in Figure 13 . This type of seal has also been used in floating ring seal applications.

Another variation is the stepped rotor seal illustrated in Figure 14. This figure shows a stepped rotor seal with a stepped stator that provides a constant clearance for each step. This type of seal has been used for the back side of an impeller and for interstage seals. It is not used very often due to problems with axial shaft travel.

The final bushing seal to be considered is the honeycomb stator seal, shown in Figure 15. This seal configuration is gaining popularity due to its leakage and rotordynamic characteristics. Typically, it is used in balance piston and interstage seal applications.

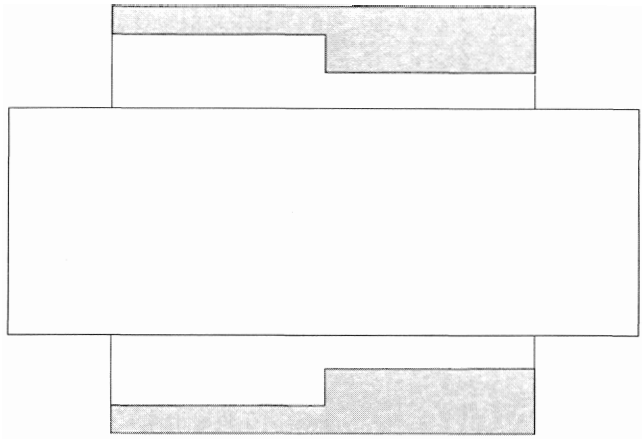

Figure 13. Example of a Stepped Bore Bushing Seal.

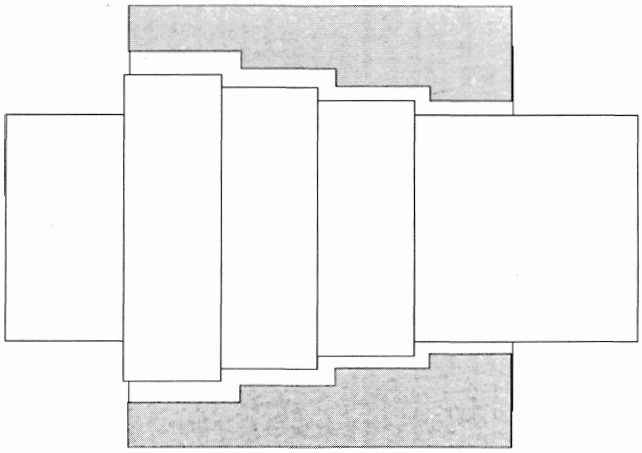

Figure 14. Example of a Stepped Rotor Bushing Seal.

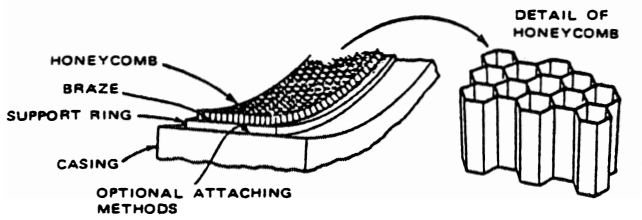

Figure 15. Example of Honeycomb Seal.

LEAKAGE CHARACTERISTICS

By definition, a seal is a device to prevent leakage of fluid from one cavity to another. Therefore, calculation of seal leakage rate is the primary objective of the seal analyst. Over the years many semiempirical relationships have been developed in an effort to accurately predict seal leakage. A few of the basic relationships are presented below, along with some design criteria based on semiempirical data.

Labyrinth Seals

The basic cavity geometry for a labyrinth seal is illustrated in Figure 16.

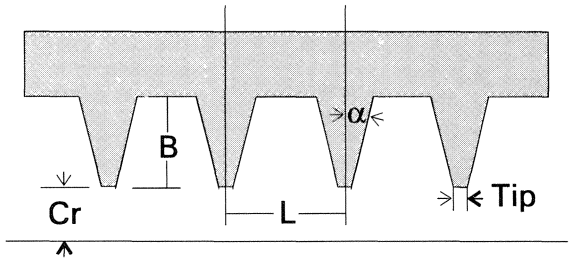

Figure 16. Labyrinth Seal Cavity.

The figure illustrates the basic parameters of radial clearance (Cr), tooth height (B), tooth pitch (L), tooth tip width (Tip), and tooth half angle (a). The other factor which significantly affects labyrinth seal leakage is the number of teeth (NT).

In the majority of cases, the clearance of a seal is selected to be larger than that of the bearings in the system. Of course, this rule is violated when abradable seals are used. The clearance is generally selected based on a radial clearance to shaft radius ratio criteria, which is typically in the range 0.002 to 0.004.

The height of a labyrinth tooth is generally selected in relation to the pitch of the teeth. Research has shown that cavities with a height to width ratio close to 1.0 have the highest drag. Since higher drag translates into lower leakage, the tooth height should be chosen to be close to the pitch of the teeth.

For straight through labyrinth seals, the optimum tooth pitch is directly dependent on the seal clearance, as illustrated in Figure 17. The figure shows that the tooth pitch to clearance ratio varies from approximately 10 to 7. For stepped and staggered seals, performance is somewhat independent of tooth pitch.

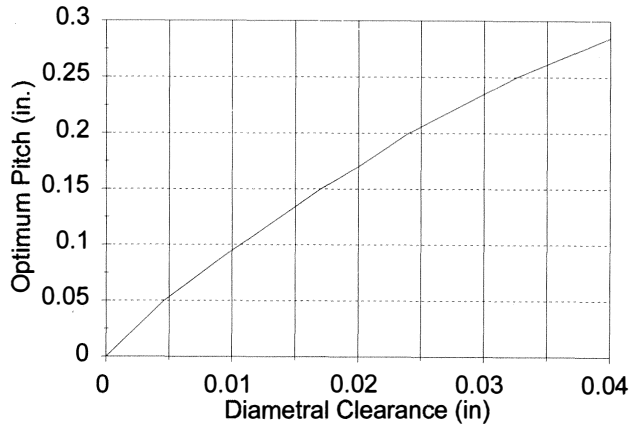

Figure 17. Optimum Pitch for See-through Labyrinth Seal.

The teeth in a labyrinth seal should be as sharp as possible for maximum loss. Typical values of tooth tip thickness are in the range of 0.005 to 0.015 in. A good rule to follow is to keep the ratio of tooth tip thickness to radial clearance less than 0.8.

The tooth half angle is typically selected for manufacturing purposes rather than leakage considerations. Ideally, the labyrinth cavity would have a leading edge, which is as straight as possible (half angle of zero) and a back side that is angled. This is why J-strips are very popular. However, most seal teeth are manufactured symmetrically for simplicity. A typical range for tooth half angle is 10 to 15 degrees.

Leakage is reduced significantly by increasing the number of teeth in a labyrinth seal. However, the effect diminishes as the number of teeth becomes large, as illustrated in Figure 18.

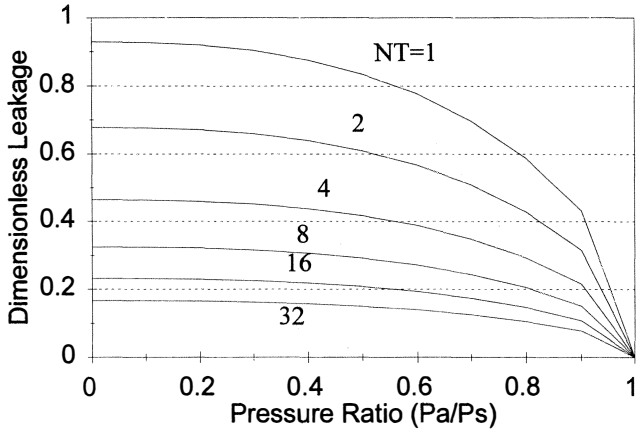

Figure 18. Leakage of Labyrinth Seal as a Function of Number of Teeth.

For staggered and stepped seals, the issue of tooth location relative to the step must be addressed. As the data in Figure 19 indicate, the tooth should be placed at the midpoint of the step for minimum leakage.

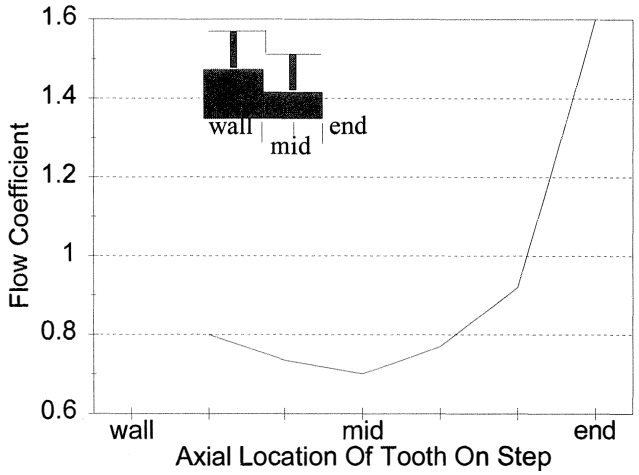

Figure 19. Effect of Tooth Location on Leakage for Stepped and Staggered Seals.

Another important parameter to be considered for stepped and staggered seals is the distance from the midpoint of the tooth to the edge of the next step. This distance is practically limited by the amount of axial shaft travel. The effect of this parameter on flow coefficient is shown in Figure 20.

Using the information given in Figures 19 and 20, the designer can determine how long the step should be and where to place the tooth. The data shown in Figure 20 could also be applied to interlocking seals.

As mentioned previously, the labyrinth seal has been the most popular annular seal. Consequently, there have also been more theories derived to predict its leakage than for any other type of seal. Presented herein is just one of many approaches for prediction of labyrinth seal leakage. The basic relationship for unchoked compressible flow through a labyrinth seal is given in Equation (1).

$$m = \mu_1 \mu_2 A \sqrt{\frac{P_s^2 - P_a^2}{NTRgt}} \qquad (1)$$

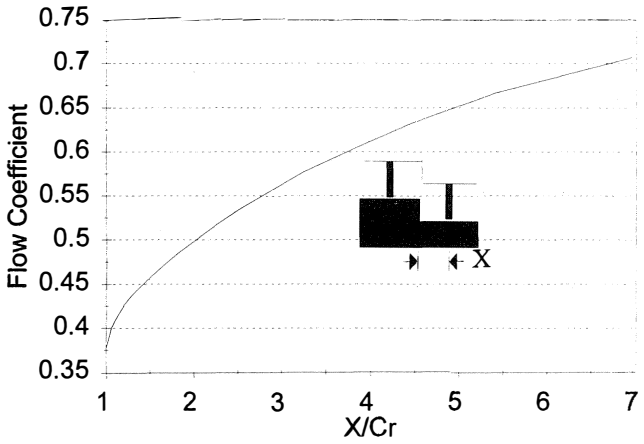

Figure 20. Effect of Tooth to Step Distance on Flow Coefficient.

There are two correction factors associated with flow through a labyrinth seal; the vena contracta (or flow coefficient) and the kinetic energy carryover coefficient, μ_1 and μ_2, respectively. The vena contracta is the apparent reduction in flow area caused by the separation streamline, as illustrated in Figure 21.

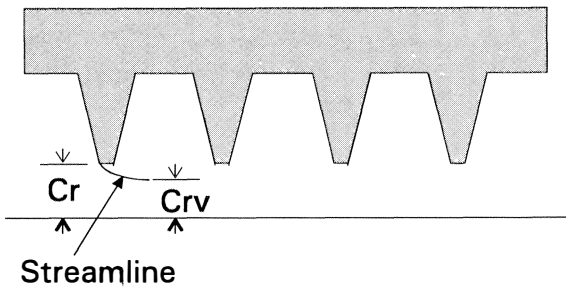

Figure 21. Vena Contracta Effect.

For compressible flow, the vena contracta effect can be defined as shown in Equation (2).

$$\mu_1 = \frac{Crv}{Cr} = \frac{\pi}{\pi + 2 - 5s + 2s^2} \tag{2}$$

where

$$s = \left(\frac{P_s}{P_a}\right)^{\frac{\gamma - 1}{\gamma}} - 1$$

When the leakage flow passes the first tooth and enters the cavity, part of the energy in the flow is converted to pressure and part remains in the jet flow and continues on to the next cavity. The kinetic energy carryover coefficient is an attempt to estimate the fraction of flow energy which is carried over to the next cavity. By definition, this coefficient has a value of 1.0 for interlocking seals. A value of unity can also be used for stepped and staggered seals. For see-through seals, the coefficient is given in Equation (3).

$$\mu_2 = \sqrt{\frac{NT}{(1 - j)\,NT + j}} \tag{3}$$

where

$$j = 1 - (1 + 16.6Cr / L)^{-2}$$

When the flow becomes choked (Mach number equals 1.0 at the last tooth), the flow across the last tooth can be expressed as:

$$\dot{m} = \frac{.510\mu_2}{\sqrt{RgT}} P_{NT-1} Cr_{NT} \tag{4}$$

where P_{NT}-1 is the pressure in the last cavity and Cr_{NT} is the radial clearance of the last tooth. For choked flow, Equations (1, 2, 3, 4) must be solved iteratively (cavity by cavity). The iterative solution method is also recommended for unchoked seals, since the flow coefficient and kinetic energy carry over coefficient may be different for each cavity. It should be noted that in a see-through labyrinth seal, the flow can only become choked at the last tooth.

Bushing Seals

The most accurate way to predict the leakage of bushing seals is to numerically integrate the film averaged continuity, momentum, and energy equations for the seal annulus, as shown below.

Continuity Equation:

$$\frac{\partial \rho UH}{\partial x} + \frac{\partial \rho VH}{\partial y} + \frac{\partial \rho H}{\partial t} = 0 \tag{5}$$

Circumferential Momentum Equation:

$$-H\frac{\partial P}{\partial x} = \tau_{rx} - \tau_{sx} + \frac{\partial \rho UH}{\partial t} + \frac{\partial \rho U^2 H}{\partial x} + \frac{\partial \rho UVH}{\partial y} \tag{6}$$

Axial Momentum Equation:

$$-H\frac{\partial P}{\partial y} = \tau_{ry} - \tau_{sy} + \frac{\partial \rho VH}{\partial t} + \frac{\partial \rho V^2 H}{\partial y} + \frac{\partial \rho UVH}{\partial x} \tag{7}$$

Energy Transport Equation:

$$C_p \cdot \left[\frac{\partial \rho HT}{\partial t} + \frac{\partial \rho HUT}{\partial x} + \frac{\partial \rho HVT}{\partial y}\right] + \frac{1}{2}\left[\frac{\partial \rho H(U^2 + V^2)}{\partial t} + \frac{\partial \rho HU(U^2 + V^2)}{\partial x} + \frac{\partial \rho HV(U^2 + V^2)}{\partial y}\right] = Q_2 + T\beta H\frac{\partial P}{\partial t} + T\beta - 1)H\left(U\frac{\partial P}{\partial x} + V\frac{\partial P}{\partial y}\right) + R\Omega\tau_{rx} \tag{8}$$

The equations of motion shown above can be applied to any of the aforementioned bushing seals, provided the proper boundary conditions are applied for steps and inlets.

When it is not feasible to integrate the equations of motion, there are some simple relationships that can be used to approximate the leakage of a plain cylindrical bore seal. For laminar flow, the relationship is given in Equation (9).

$$\dot{m} = \frac{\pi R C r^3}{6\mu L R g T}\left(Ps^2 - Pa^2\right) \tag{9}$$

For turbulent flow the relationship is given in Equation (10).

$$\dot{m} = 2\pi R K C r^{\frac{3}{2-n}} \tag{10}$$

where

$$K = \left(\frac{2^2 + n\left(Ps^2 - Pa^2\right)}{mLRgT\mu^n}\right)^{\frac{1}{2-n}}$$

and n and m are defined by the following friction factor relationship.

$$f = m\,Re^n$$

where the Reynolds number is defined as:

$$Re = \frac{2\dot{m}}{\pi D \mu}$$

For smooth seals, typical values of m and n are 0.316 and -0.25, respectively.

The main factor, other than clearance, which controls cylindrical seal leakage is the stator roughness. The effect of stator roughness on leakage is illustrated in Figure 22. The large values of stator roughness (>0.02) shown in the figure are only achievable by using patterns such as round holes and diamond knurls. While rotor roughness may also reduce leakage, it has a detrimental effect on rotordynamics.

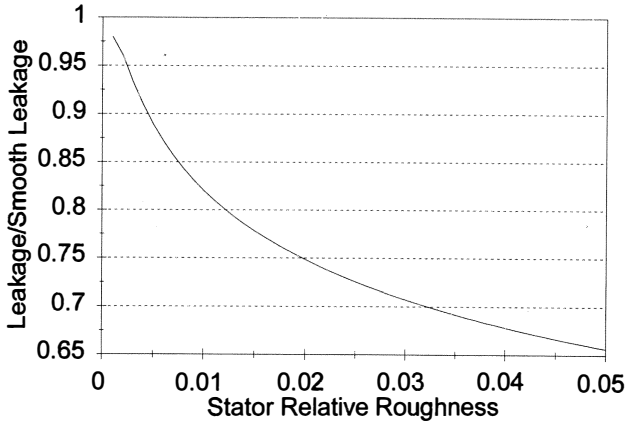

Figure 22. Effect of Stator Roughness on Seal Leakage.

While simple relationships are not very accurate for tapered bore seals, Equations (9) and (10) can be used for a first approximation by using the average radial clearance in the equations.

For stepped bore seals, the relationships given in Equations (9) and (10) can be utilized by substituting the pressure at the step for the supply pressure, P_s. Referring to Figure 23, the pressure at the step, P_{step}, can be calculated as shown in Equation (11).

$$P_{step} = p_a^2 \frac{\left(\frac{P_s}{P_a}\right)^2 + \frac{1-b}{b}\left(\frac{Cr_{min}}{Cr_{max}}\right)^3}{1 + \frac{1-b}{b}\left(\frac{Cr_{min}}{Cr_{max}}\right)^3} \tag{11}$$

where

$$b = X_1 / X_2$$

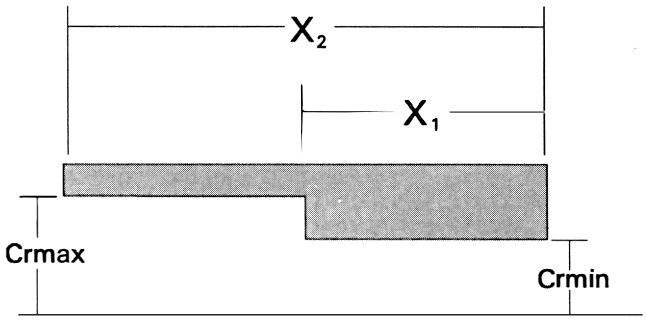

Figure 23. Stepped Bore Seal.

The leakage characteristics of a typical seal calculated using the relationships given in Equation (11) are shown in Figure 24. The figure illustrates the fact that as the clearance increases and effective length decreases, the leakage increases.

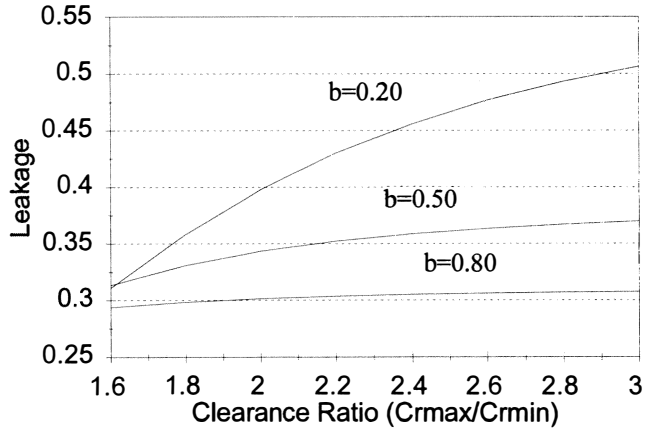

Figure 24. Leakage Characteristics for Stepped Bore Seal.

The leakage characteristics of the stepped rotor bushing seal can only be accurately predicted by numerically solving the equations of motion.

Finally, the question of eccentric operation often arises when discussing bushing seals. For laminar flow, the following relationship can be used to estimate the effect of eccentricity on seal leakage:

$$\frac{\dot{m}_{ecc}}{\dot{m}_{cen}} = 1 + \frac{3e^2}{2Cr^2} \tag{12}$$

For turbulent flow, the expression (Equation 13) becomes much more complicated and can not be solved in a closed form.

$$\frac{\dot{m}_{ecc}}{\dot{m}_{cen}} = \frac{1}{\pi}\int_0^{\pi}\left(1 - \frac{e}{Cr}\cos\theta\right)^{12/7} d\theta \qquad (13)$$

The results for both laminar and turbulent flow are shown in Figure 25. As expected, the figure shows that as seals become eccentric, the leakage increases.

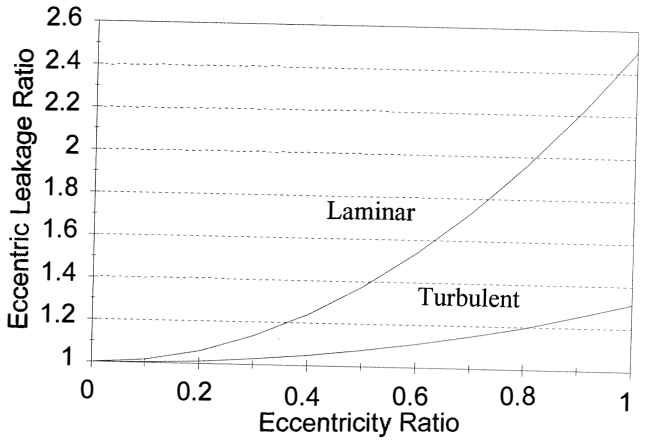

Figure 25. Effect of Eccentricity on Bushing Seal Leakage.

The last type of bushing seal to be considered is the honeycomb stator seal. There have been several approaches proposed for predicting the leakage of a honeycomb seal: consider the foils to be like labyrinth teeth, apply an empirical relationship to a Bernoulli type of equation, or treat the honeycomb surface as a roughened stator for a bushing seal. All of the options are addressed here.

If the honeycomb seal is considered to be similar to a labyrinth seal, the approach is very straight forward. The honeycomb cell characteristics of depth, width, and foil thickness replace the labyrinth teeth characteristics of height, pitch, and tip width. The labyrinth seal leakage equations presented above (Equation 1) are then applied directly.

An empirical relationship for honeycomb leakage is given in Equation (14).

$$\dot{m} = A\sqrt{\frac{P_s^2 - P_a^2}{RgT\left[1.5 + 1.5(ncl - 1)\right]}} \qquad (14)$$

where ncl is the number of cell walls.

Yet another approach is to consider the honeycomb to be a rough stator. This approach is not preferable because extensive testing has indicated that flow over a honeycomb surface does not behave like flow over a rough surface. None the less, there have been many tests conducted for honeycomb seals and some friction factor data is available. A sample of data for use in Equation (10) is given in Table 1.

A comparison is shown in Figure 26 of the various methods of calculating honeycomb seal leakage with test data. The figure shows that the best method is to calculate the leakage using the relationships for a labyrinth seal given in Equation (1). The next best approach is the empirical relationship given in Equation (14). The least attractive method is to consider the seal to be a rough bushing. A better rough bushing estimate can be obtained by integrating the equations of motion (Equations 5, 6, 7, 8). However, the roughness approach to predicting honeycomb seal leakage is only effective for seal configurations that have been tested in advance to obtain friction factor data at the operating condition of interest. These data are not likely to be available for new seal designs operating in process conditions. The labyrinth seal approach yields consistently accurate results without requiring testing of the seal in advance.

Table 1. Honeycomb data for friction factor calculation.

Cell Width	Cell Depth	m	n
.020 in	.058 in	1.696	-.134
.062 in	.058 in	0.62	-.098
.062 in	.075 in	1.212	-.117

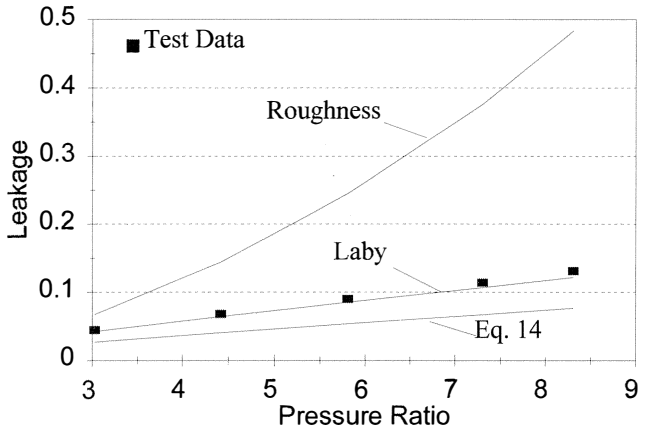

Figure 26. Honeycomb Seal Leakage Calculated by Various Methods.

When designing a honeycomb seal, the most important consideration is strength. The brazing material, method of construction, foil material, and foil thickness must be chosen to ensure structural integrity under high pressure conditions.

Typical foil materials are stainless steel, Inconel, and Hastelloy. The material chosen should be compatible with the process gas, suitable for the operating temperatures, and have a hardness less than that of the shaft. If possible, the foils should be bonded using a braze foil process. This results in the highest bond strength. Typical foil thicknesses are given in Table 2.

A summary comparison is shown in Figure 27 of leakage for the different types of seals described above for a generic operating condition and geometry. Note that the best see-through seal designs are the slant tooth labyrinth and the honeycomb stator bushing seal.

Table 2. Typical honeycomb seal foil thicknesses.

Cell Width	Foil Thickness
1/16 in	0.002-0.005 in
1/8 in	0.004-0.008 in
3/16 in	0.006-0.015 in

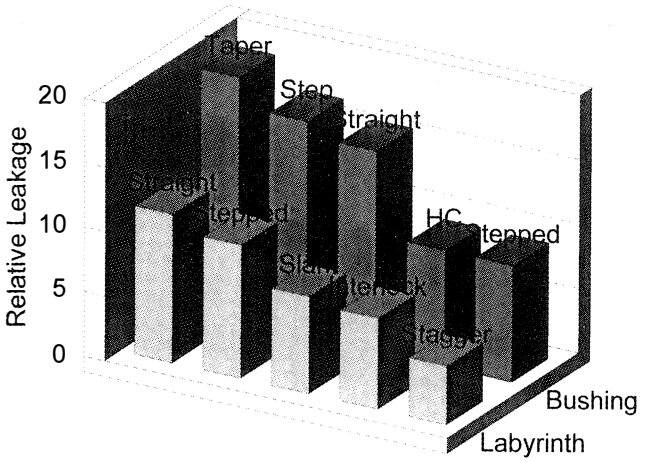

Figure 27. Leakage Comparison for Various Seal Configurations.

DYNAMIC CHARACTERISTICS

When pressure is applied across a seal, the fluid accelerates as it enters the seal and a separation region forms that results in a localized pressure drop. This pressure drop is typically described by a relationship similar to the one given in Equation (15).

$$\Delta P_{ent} = \frac{1}{2}\ \rho V^2(1 + \xi) \tag{15}$$

where x is the entrance loss coefficient which typically varies between 0 and 0.5. For a seal operating in the concentric position, this drop in pressure is uniform around the circumference. However, when the seal becomes slightly eccentric (as shown in Figure 28) the fluid velocity is not uniform about the circumference of the seal. This results in a larger pressure drop on the side of the seal with a larger local clearance and a smaller pressure drop on the side of the seal with a smaller local clearance. Consequently, a force imbalance is created that acts to restore the shaft to the center of the seal. It should be remembered that the basic operating principle described above assumes that the seal will have a positive direct stiffness. However, there are operating conditions such as a small pressure drop combined with a very high speed which can lead to a negative direct stiffness and labyrinth seals typically have a negative direct stiffness.

When the shaft inside of a seal starts to rotate and whirl (as all shafts do), the fluid film forces acting on the shaft become more complicated. A whirling shaft with fluid film forces acting on it is illustrated in Figure 28. The figure shows that both radial (restoring) and circumferential forces are generated by the fluid film. For convenience, these forces can be expressed in terms of force coefficients (stiffness and damping) as shown in the following linearized equations of motion:

$$-\begin{Bmatrix} F_x \\ F_y \end{Bmatrix} = \begin{bmatrix} K_{xx} & K_{xy} \\ K_{yx} & K_{yy} \end{bmatrix} \begin{Bmatrix} x \\ y \end{Bmatrix} + \begin{bmatrix} C_{xx} & C_{xy} \\ C_{yx} & C_{yy} \end{bmatrix} \begin{Bmatrix} \dot{X} \\ \dot{y} \end{Bmatrix} \tag{16}$$

In Equation (16), (X,Y) define the motion of the rotor relative to its steady-state arbitrary position; are the components of the reactive force acting on the rotor; and (K,C) are stiffness and damping, respectively. Inertia coefficients (M) are considered negligibly small for compressible flow seals.

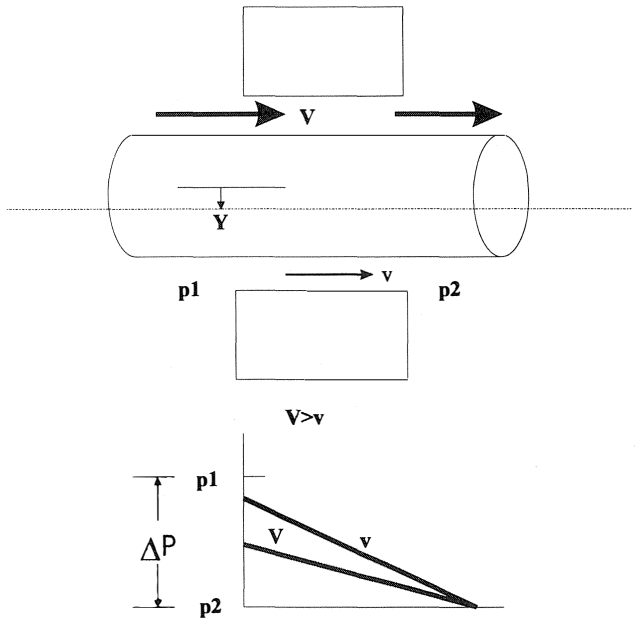

Figure 28. Force Generating Phenomenon of an Annular Seal.

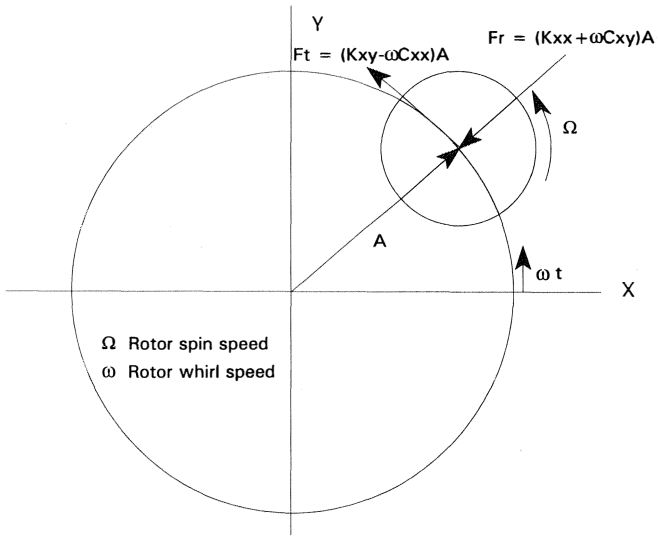

Figure 29. Forces Acting on a Whirling Shaft.

For seals operating in the concentric position, the rotordynamic coefficients can be considered to be skew-symmetric. Therefore, Equation (16) can be rewritten as:

$$-\begin{Bmatrix} F_x \\ F_y \end{Bmatrix} = \begin{bmatrix} K & k \\ -k & K \end{bmatrix} \begin{Bmatrix} x \\ y \end{Bmatrix} + \begin{bmatrix} C & c \\ -c & C \end{bmatrix} \begin{Bmatrix} \dot{X} \\ \dot{y} \end{Bmatrix} \tag{17}$$

The aforementioned restoring force yields a stiffness component that acts much like the stiffness of a bearing. The seal stiffness must be included in the rotordynamic analysis model in order to obtain accurate natural frequency predictions.

The manner in which annular seals affect rotordynamic stability can be explained as follows: The circumferential force, Ft, shown in Figure 28, is caused by the fluid traveling around the circumference of the shaft at a frequency that is generally different than the frequency of rotation. Much like the response of the shaft due to the force of mass imbalance, when the frequency at which the fluid is traveling about the circumference is the same as a natural frequency of the system, the amplitude

of shaft vibration increases dramatically. The relationship between natural frequency and shaft rotational frequency at which this amplification will occur for a particular fluid film element is typically expressed as the whirl frequency ratio;

$$WFR = \frac{k}{\omega \pi C} \tag{18}$$

where k is the cross-coupled stiffness and C is the direct damping of the fluid film element. For fluid elements such as plain sleeve bearings this number is very close to 0.5 giving rise to the term half speed whirl. This term comes from the observation that a rotor system with sleeve bearings would tend to experience whirl (a large amplitude response at a frequency other than shaft speed) when the shaft rotation frequency reached twice that of the first natural frequency. The whirl frequency ratio for gas seals is typically less than 1.0; however, there are instances where it can be greater than 1.0. In general, the smaller the whirl frequency ratio the better.

The tendency for the whirl frequency ratio of gas seals to be less than 1.0 indicates that the effects of gas seals on the rotordynamic stability of a turbomachine may only be of concern when the turbomachine of interest is operating above its first natural frequency. However, for long seals under high pressure, the direct stiffness of the seal will affect the first mode frequency. In the case of labyrinth balance piston seals, the direct stiffness is a large negative value that would tend to lower the first natural frequency.

As discussed above, the forces acting on the shaft are directly a function of the pressure distribution along the length of the seal. Therefore, all effects that influence pressure distribution (clearance profile, roughness, etc.) also influence the rotordynamic coefficients. Generalized results are presented in Figure 30 for the influence of pressure drop on the rotordynamic coefficients: direct stiffness, cross coupled stiffness, and direct damping. The figure shows that the coefficients generally increase linearly with pressure drop.

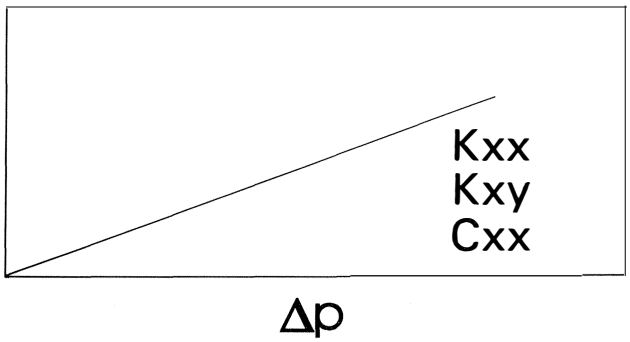

Figure 30. Influence of Pressure Drop on Rotordynamic Coefficients.

The influence is shown in Figure 31 of shaft speed on the rotordynamic coefficients: direct stiffness, cross coupled stiffness, and direct damping. The figure shows that direct stiffness is somewhat constant with speed and then tends to decrease slightly. Substantial decreases in stiffness only occur for very high speed conditions. The figure also shows that cross coupled stiffness increases with an increase in shaft speed. The figure shows a zero cross coupled stiffness at zero speed because the influence of inlet swirl is neglected. Finally, the figure shows that direct damping increases slightly as speed increases.

For rotordynamics, the objective in designing an annular seal for a high performance turbomachine should be to minimize the

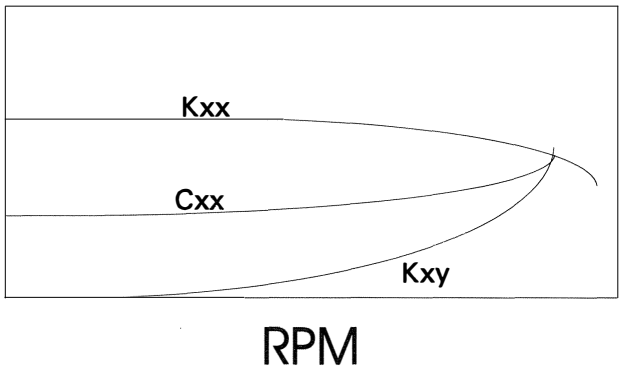

Figure 31. Influence of Shaft Speed on Rotordynamic Coefficients.

whirl frequency ratio. In order to do so, the characteristics of the two dominant terms (see Equation 18); the cross coupled stiffness and direct damping, should be understood. Referring to Figure 29, both terms are derived from the circumferential force acting on the rotor surface. Therefore, both are influenced to some degree by the circumferential velocity in the seal. Generalized characteristics of cross coupled stiffness and direct damping are shown in Figure 32 as a function of inlet swirl. The figure shows that cross coupled stiffness is a linear function of inlet swirl and that direct damping is somewhat influenced by large values of inlet swirl.

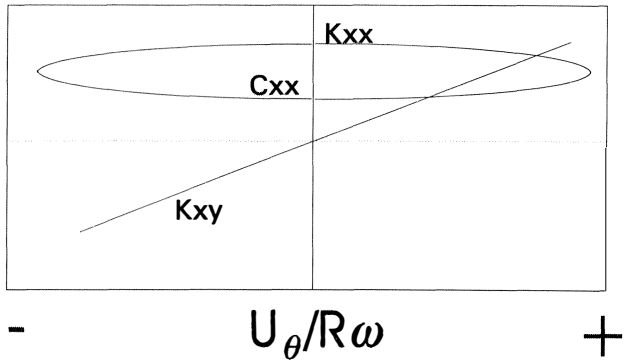

Figure 32. Influence of Inlet Swirl on Rotordynamic Coefficients.

A conclusion that can be drawn from these illustrations is that the whirl frequency ratio is a somewhat linear function of inlet swirl. Therefore, limiting the inlet swirl improves the rotordynamic stability characteristics of annular seals. Inlet swirl can be minimized through the use of devices at the inlet to an annular seal which reduce the inlet swirl known as swirl brakes. However, whether or not swirl brakes can be used, a reasonable estimate of inlet swirl must be used as input to the analysis in order to establish a boundary condition for the solution method. If values can not be obtained from analysis of the fluid flow in the machine, the values given in Table 3 should be used as guidelines.

Another significant influence on the rotordynamic characteristics of annular seals is surface roughness. With respect to bushing seals, substantial benefits are obtained from surface roughness of the stator. The roughness of the stator increases surface shear stress that results in a net decrease in the circumferential velocity of the fluid inside the seal. The distribution of fluid circumferential velocity inside a bushing seal is illustrated in Figure 33.

The figure shows that for the same value of inlet swirl, the circumferential velocity of a seal with a smooth stator and

Table 3. Recommended Inlet Swirl Values.

Seal Type	Inlet Swirl
With Swirl Brakes	0.1 - 0.3
Interstage Seal	0.5 - 0.7
Eye/Balance Piston Seal	0.6 - 1.0

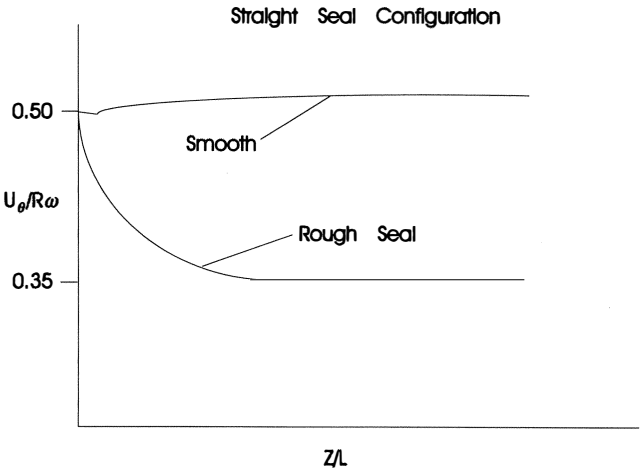

Figure 33. Circumferential Velocity Distribution Inside a Bushing Seal.

smooth rotor increases slightly prior to achieving its asymptotic value while that of a seal with a rough stator and smooth rotor decreases significantly prior to achieving its asymptotic value. This decrease in the circumferential velocity due to increased stator surface roughness results in a net decrease in cross coupled stiffness and a net increase in direct damping, as shown in Figure 34. Therefore, the value of whirl frequency ratio is decreased resulting in improved rotordynamic stability characteristics.

A somewhat overlooked characteristic of annular seals is the direct stiffness. Annular seals function in a manner similar to hydrostatic bearings and can significantly influence the natural frequencies of turbomachines. With the right boundary conditions, bushing seals can even replace conventional bearing configurations. Stiffness is directly influenced by pressure drop,

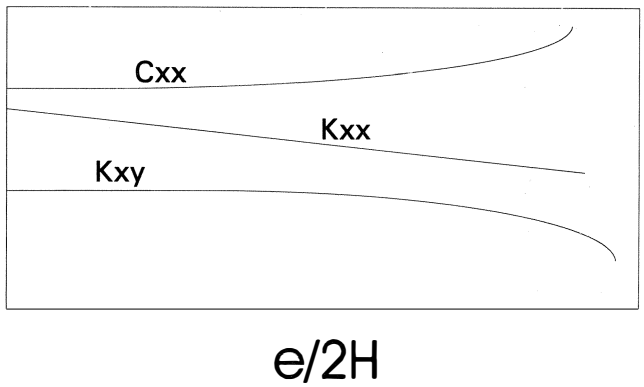

Figure 34. Influence of Stator Roughness on Rotordynamic Coefficients.

which should be expected, as shown in Figure 30. Speed, inlet swirl, and roughness affect stiffness, but only slightly, as shown in Figures 31, 32, and 34. Other than pressure drop, theoretically the most significant influence on stiffness is clearance. Specifically, theory predicts that a tapered clearance profile will significantly increase direct stiffness. This effect is illustrated in a general manner in Figure 35. The figure shows that an optimized value of direct stiffness can be obtained when the inlet clearance is larger than the exit clearance. A typical range of values for this ratio at the optimum stiffness point is 2.5 to 3.0. This effect has been shown experimentally for compressible flow seals. In general, it is good practice to design annular seals with a slight taper to prevent divergence of the clearance that may lead to rapid degradation in rotordynamic characteristics and to accommodate wear. Referring again to Figure 35, it is clear that increasing clearance taper will result in a rapid increase in the whirl frequency ratio, since cross coupled stiffness will increase and direct damping will decrease.

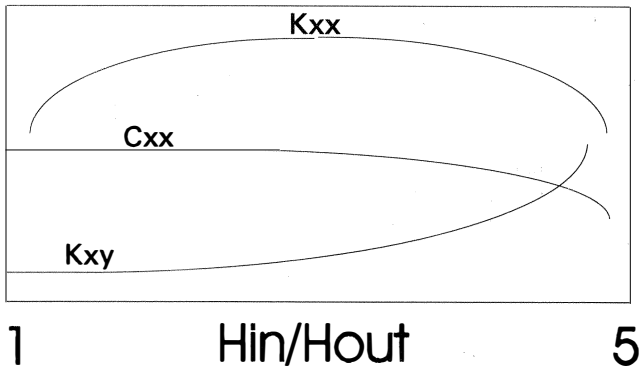

Figure 35. Influence of Clearance Taper on Rotordynamic Coefficients.

Other factors that influence stiffness are seal length and seal diameter. Generally, stiffness will increase with increasing length. However, due to the influence of circumferential velocity in the clearance, there is an optimum seal length for maximum stiffness. For many instances, the general profile of the curves shown in Figure 35 could be used for seal length along with clearance taper. The primary difference being that the optimum length for maximum stiffness is a strong function of shaft speed, inlet swirl, and stator surface roughness. The influence of seal diameter on rotordynamic coefficients has the same characteristics as those shown in Figure 30 for pressure drop. The rotordynamic coefficients increase as diameter increases. In many cases, changes in rotordynamic coefficients as a function of diameter can be estimated by multiplying by the ratio of the diameters (for small changes).

As mentioned previously, all shafts whirl. Similarly, all shafts operate somewhat eccentrically in the seal bore, due to applied loads and fluid film forces. In general, seal performance (other than leakage) does not change significantly for eccentricity ratios (eccentricity divided by radial clearance) in the range 0-0.50. Therefore, a solution for a centered seal can be used in many instances. Typical characteristics of direct stiffness as a function of shaft eccentricity (in the x-direction) for a bushing seal are shown in Figure 36. The main trend shown in Figure 36 of the magnitude of stiffness increasing with eccentricity holds as well for labyrinth seals. The only difference being that labyrinth seal stiffness is typically a negative value.

The influence of shaft eccentricity on cross coupled stiffness for a bushing seal is shown in Figure 37. The figure shows that

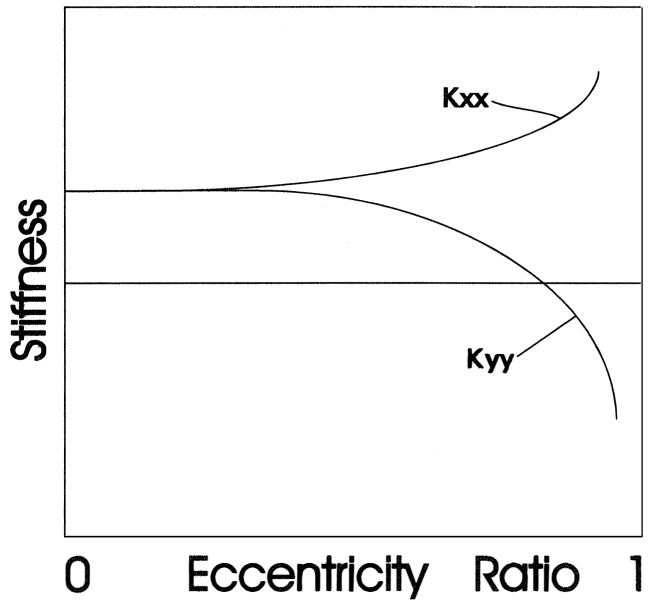

Figure 36. Influence of Shaft Eccentricity on Direct Stiffness.

the magnitude of cross coupled stiffness increases as eccentricity increases. The same trend holds for labyrinth seals.

The influence is reflected in Figure 38 of shaft eccentricity on direct damping for a bushing seal. The figure shows that the magnitude of direct damping increases as eccentricity increases. For labyrinth seals, the trend is quite different; damping increases slightly for small values of eccentricity and then decreases sharply as eccentricity becomes large. This trend, combined with the cross coupled stiffness, results shown in Figure 37 would indicate that the whirl frequency ratio of a labyrinth seal may increase dramatically as eccentricity increases, while that of a bushing seal may stay relatively the same, depending on the seal configuration and operating conditions.

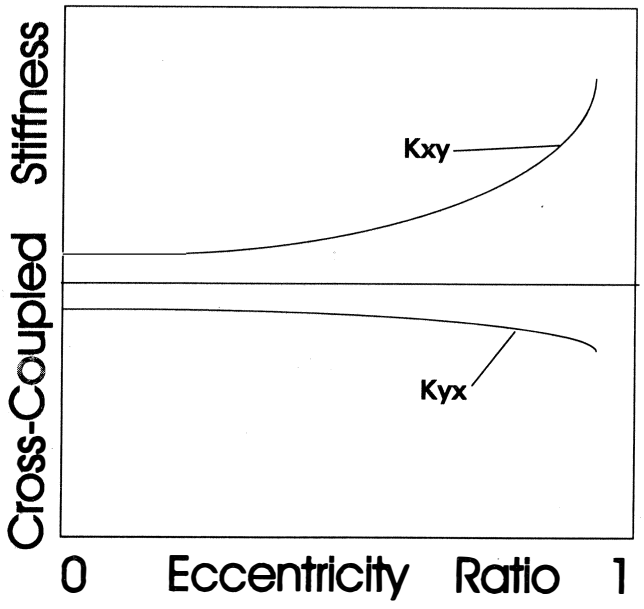

Figure 37. Influence of Shaft Eccentricity on Cross coupled Stiffness.

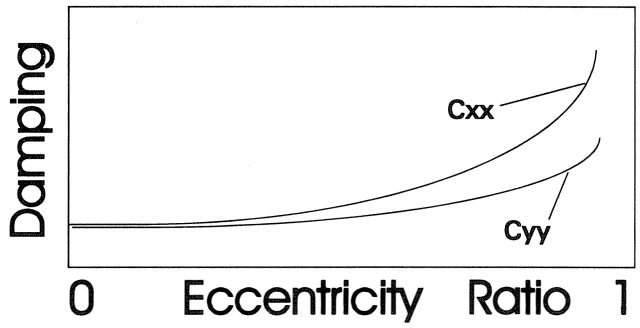

Figure 38. Influence of Shaft Eccentricity on Direct Damping.

Labyrinth Seals

Existing analysis techiques for determination of labyrinth seal rotordynamic coefficients is not quite sophisticated enough to accurately predict the influence of features such as tooth half angle, tooth tip width, cavity geometry, etc., on stiffness and damping. Some researchers have made attempts at such analyses, but their findings have yet to be validated experimentally. The discussion presented below is based mainly on analytical predictions. When available, results based on experimental data are used.

Analytical predictions for teeth on stator see-through labyrinth seals have shown that milled teeth (those with a tooth half angle greater than 0) will yield a higher stiffness and a lower WFR than J-strips.

Test data have indicated that staggered labyrinth seals have a much larger magnitude of negative direct stiffness and a much lower WFR than teeth on stator see-through seals.

Predictions are shown in Figure 39 for the direct stiffness of see-through and stepped labyrinth seals as a function of tooth location (TOR=teeth on rotor, TOS=teeth on stator) and number of teeth. The figure shows that teeth on rotor seals can have a more positive value of stiffness than teeth on stator seals and that the stiffness becomes more positive as the seal becomes more divergent.

Data are shown in Figure 40 for the whirl frequency ratio (WFR) for the same conditions and configurations of labyrinth seals. The figure shows that at the seal becomes more divergent, the WFR decreases. This is expected, since the WFR is dependent on circumferential velocity in the seal, and as the diameter

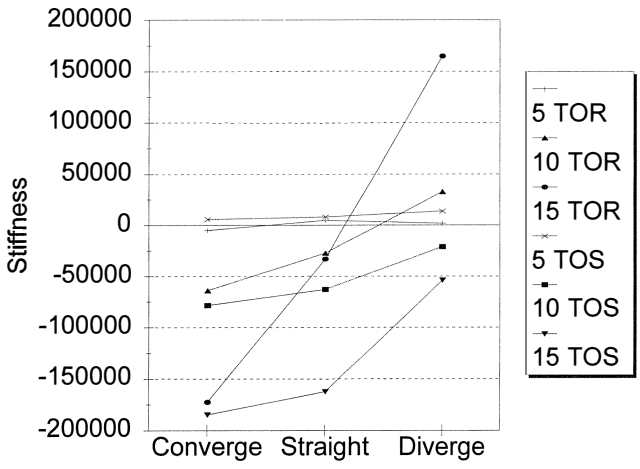

Figure 39. Stiffness for Stepped and See-through Seals as a Function of Number of Teeth and Tooth Location.

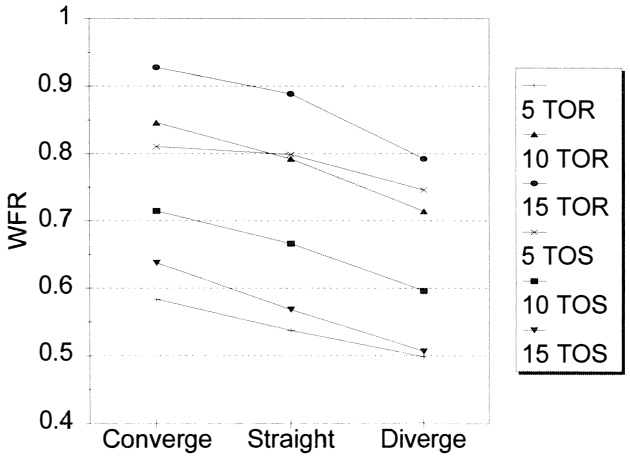

Figure 40. Wfr for Stepped and See-through Seals as a Function of Number of Teeth and Tooth Location.

of the rotor increases the circumferential velocity decreases due to conservation of angular momentum. The figure also indicates that teeth on stator seals have a lower WFR than teeth on rotor seals. While this may be true for this particular case, the relative performance of TOR and TOS seals is highly dependent on operating conditions and geometry.

Generally, labyrinth seals have rotordynamic characteristics that are detrimental to the stability of high speed, high pressure turbomachines. In an effort to minimize the detrimental effects of labyrinth seals, two approaches have been tried: swirl brakes and shunts.

A swirl brake is a device that is inserted at the entrance to a seal in an effort to decrease the circumferential velocity entering the seal. Swirl brakes can be as simple as a flat ring with radial slots milled into the face or as complicated as an aerodynamically designed ring with miniature air foils to turn the flow. Either configuration is acceptable and both have demonstrated the desired result: lower cross coupled stiffness.

Another approach is to us a shunt, as illustrated in Figure 41. A shunt is merely the injection of high pressure fluid at an intermediate point along the seal at one or more circumferential locations. The idea is that the injected fluid will break up the circumferential flow in the seal and reduce the cross coupled stiffness. The most effective shunts inject the fluid against the direction of shaft rotation, as shown in the figure.

While both swirl brakes and shunts are effective at reducing labyrinth seal cross-coupled stiffness and consequently improving the rotordynamic stability of the turbomachine, they both have drawbacks. Both the shunt and swirl brake do not affect the negative direct stiffness or low direct damping of a labyrinth seal. In addition, the shunt effectively shortens the seal, which results in an increase in seal leakage which translates into a decrease in machine efficiency.

Finally, one could surmise from the introduction of this section on dynamic characteristics that the introduction of roughness on the stator would improve the rotordynamic characteristics of seals in general. This is an appealing thought since rough surfaces such as honeycomb have been used extensively with seals having labyrinth teeth on the rotor. However, test data have shown that introduction of a rough surface such as honeycomb on the stator portion of a tooth on rotor labyrinth seal has not resulted in an improvement in the whirl frequency ratio.

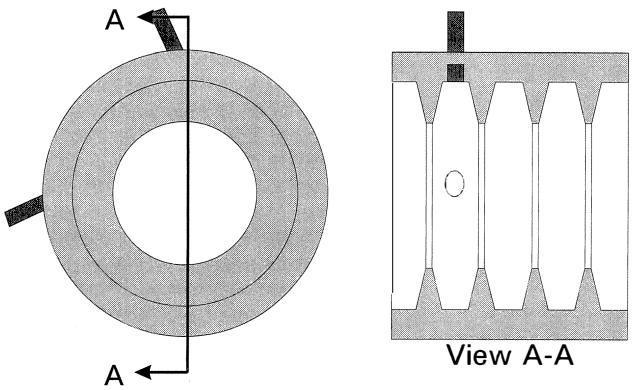

Figure 41. Example of a Shunt.

Bushing Seals

The previous discussion of general seal characteristics presented at the beginning of this section adequately covered cylindrical and tapered bushing seal characteristics. The following information pertains to other configurations such as stepped bore, multistepped, and honeycomb.

Results for stepped bore seal stiffness as a function of radial clearance ratio and step length are shown in Figure 42. The figure shows that, like the tapered seal, there is an optimum clearance ratio for maximum stiffness and as the step length is increased, stiffness increases.

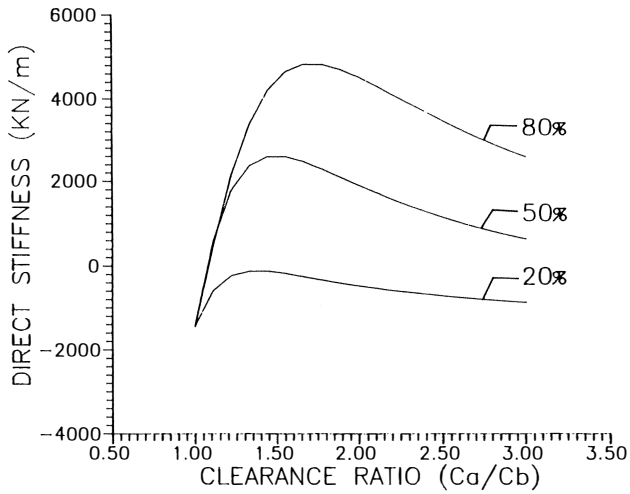

Figure 42. Step Seal Stiffness as a Function of Clearance Ratio and Step Length.

While the results presented in Figure 42 are typical of stepped bore seals, slight changes in geometry can lead to large changes in stiffness characteristics. Results shown in Figure 43 are for the same conditions as those presented in Figure 42, except that the length of the seal has been shortened. Instead of a maximum stiffness value, the figure shows that a minimum is obtained when clearance ratio is increased and that the largest magnitude occurs for the longest step length.

The whirl frequency ratio results are shown in Figures 44 and 45 for the same conditions as those used in Figures 42 and 43, respectively. The figures show that stepped bore seals have lower values of WFR than cylindrical bore seals and that the WFR tends to decrease as clearance ratio is increased. In the case of the shorter seal, Figure 45, a minima is reached at a clearance ratio of 1.5.

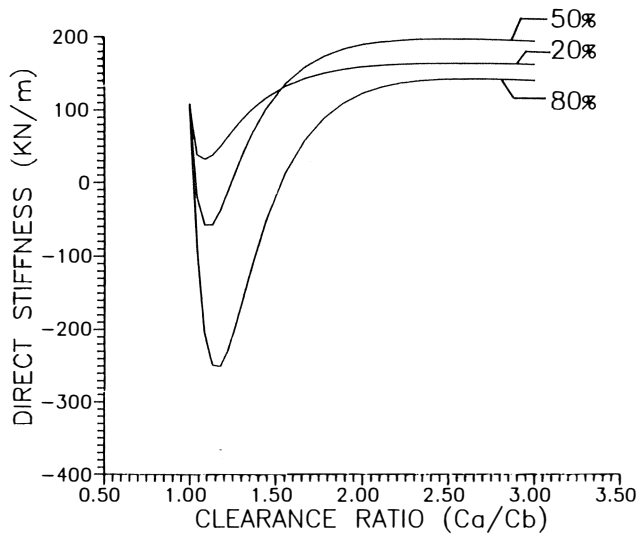

Figure 43. Step Seal Stiffness as a Function of Clearance Ratio and Step Length for a Shorter Seal.

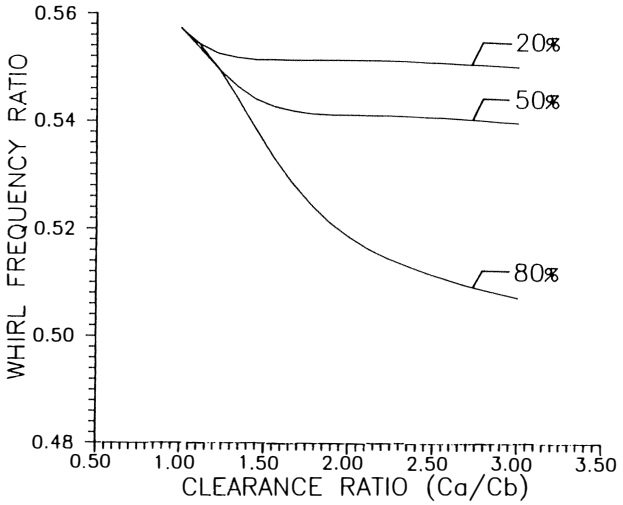

Figure 44. Step Seal Wfr as a Function of Clearance Ratio and Step Length.

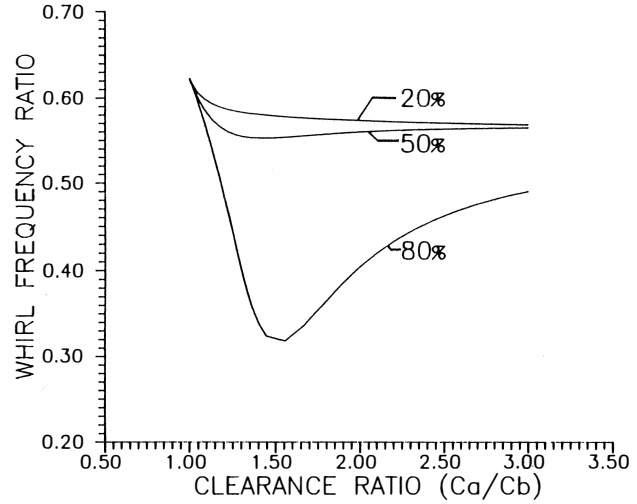

Figure 45. Step Seal Wfr as a Function of Clearance Raio and Step Length.

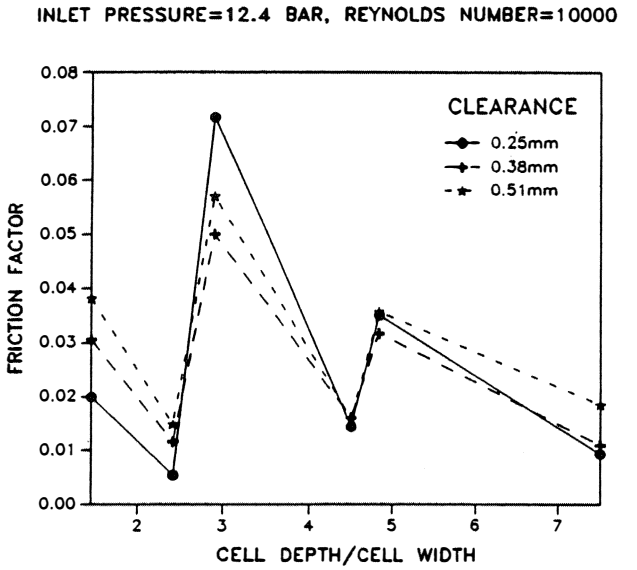

Figure 46. Honeycomb Phenomenon (HA, 1989). Friction Factor Jump in a Honeycomb Seal.

By far the most rotordynamically significant bushing seal is the honeycomb. The characteristics of honeycomb seals that result in favorable rotordynamic characteristics are the roughness of the surface and the action of the fluid within the cell. The effects of roughness on rotordynamic characteristics were adequately discussed in the introduction to this section. The energy dissipating characteristics of the honeycomb cell are dependent on cell volume, fluid properties, and Reynolds number of the flow. When combined, these effects cause nonlinear phenomena such as a jump in friction factor, illustrated in Figure 46. Large energy dissipation results in large values of direct damping and a reduction in cross coupled stiffness.

A comparison is given in Figure 47 of honeycomb seal stiffness with a smooth (cylindrical bore) bushing seal along with a labyrinth seal. The figure shows that the honeycomb seal has a positive direct stiffness which is comparable to that of a smooth bore seal.

The WFR results for the same data set are shown in Figure 48. The figure shows that the honeycomb seal has a substantially smaller WFR than that of either the labyrinth seal or the smooth bore seal. While both the WFR and stiffness results show the beneficial characteristics of the honeycomb seal, the real value is the large magnitude of damping.

A comparison of direct damping for the same data set is shown in Figure 49. The figure shows that the damping of a honeycomb seal can be extremely large. When placed at a critical location such as a balance piston seal, this damping can significantly improve the rotordynamic characteristics of an entire system both in terms of stability and synchronous response.

The effects of seals on the rotordynamics of a turbomachine can be illustrated using the following results for a back to back multistage centrifugal compressor. The original configuration of the compressor had a staggered labyrinth balance piston seal and tilt pad bearings. The rotordynamic analysis results for this configuration are shown in Table 4. The data show that the baseline rotordynamic analysis from the manufacturer (no seals) shows a positive logarithmic decrement (large damping in system which means stable operation). However, when labyrinth

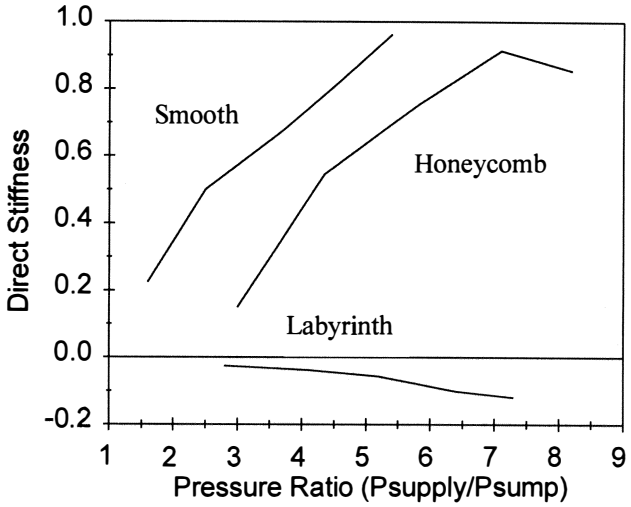

Figure 47. Direct Stiffness Comparison of Honeycomb, Smooth, and Labyrinth Seals.

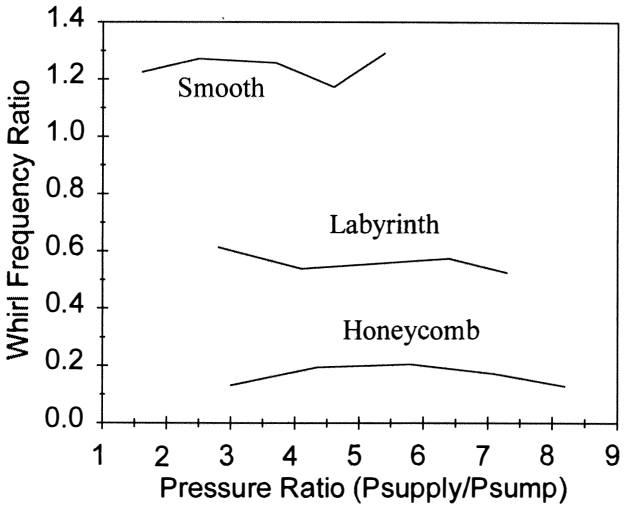

Figure 48. Wfr Comparison of Honeycomb, Smooth, and Labyrinth Seals.

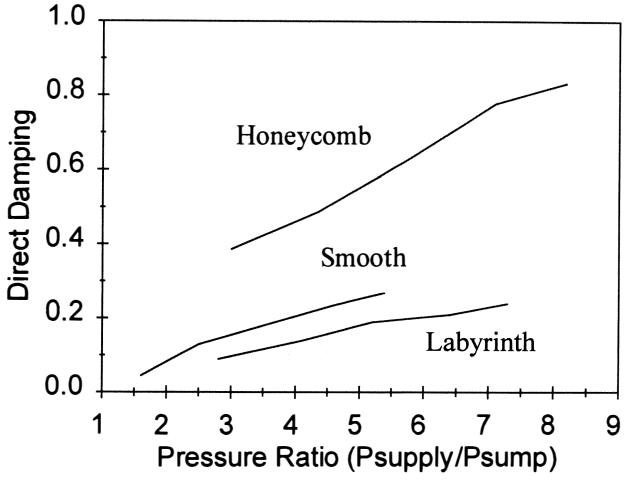

Figure 49. Direct Damping Comparison of Honeycomb, Smooth, and Labyrinth Seals.

Table 4. Compressor Stability Assessment

FIRST FORWARD MODE LOG DEC AT 10,500 RPM			
	Original Bearing	Optimized Bearings	Lobed Bearing (2 Lobes)
ROTORDYNAMIC ANALYSIS	Log Dec (-)	Log Dec (-)	Log Dec (-)
BEARINGS ONLY	0.407	0.65	-0.713
ADDING SEALS	-0.320	-0.037	-1.355
CHANGE TO HONEYCOMB	2.472	2.913	1.141

seal analysis tools are applied to the problem, the logarithmic decrement for the machine becomes negative (unstable operation). The manufacturer's approach to the problem was to optimize the (tilting pad) bearings. The data show that this does little to improve the stability of the machine (logarithmic decrement is still negative). However, application of honeycomb damping seals improve the machine stability characteristics tremendously (large positive logarithmic decrement). In addition, the honeycomb damping seal would even enable the use of simpler, lower cost bearings (2-lobe) in the machine at a savings of thousands of dollars per machine. This example is included to illustrate that a seal modification can be as effective or more effective than a bearing modification.

NOMENCLATURE

A	seal leakage area
B	labyrinth tooth height
C	direct damping, damping
Cr	radial clearance
D	diameter
F	force
H	radial clearance function
K	direct stiffness, stiffness
L	length or tooth pitch
NT	number of teeth
P	pressure
R	radius
Rg	gas constant
Qs	heat
T	temperature
Tip	labyrinth tooth thickness
U	axial velocity
V	velocity (circumferential)
X	displacement
Y	displacement
b	step length ratio
c	cross-coupled damping
e	eccentricity
f	friction factor
k	cross coupled stiffness
$\dot{m}$	mass flowrate
ncl	number of honeycomb foils
v	velocity
t	time
Ω	shaft speed
α	tooth half angle
β	compressibility factor
γ	ratio of specific heats
μ	fluid viscosity
μ_1	flow coefficient
μ_2	kinetic energy carryover coefficient
ρ	fluid density
τ	shear stress
ξ	entrance loss coefficient

Subscripts

NC	last labyrinth seal cavity
NT	last labyrinth seal tooth

a	ambient (as in pressure)
cen	centered value
ecc	eccentric value
ent	entrance region value
r	rotor value or radial component
s	supply or stator value
step	at the step location
t	tangential component
v	at the vena contracta
x	x-direction
y	y-direction

BIBLIOGRAPHY

Childs, D. W. and Scharrer, J. K., "Experimental Rotordynamic Coefficient Results for Teeth-On-Rotor and Teeth-On-Stator Labyrinth Gas Seals," ASME Journal of Engineering for Gas Turbine and Power, *108*, pp. 599-604 (1986).

Childs, D. W. and Scharrer, J. K., "Theory Versus Experiment for the Rotordynamic Coefficients of Labyrinth Gas Seals: Part II - A Comparison to Experimental Results," ASME Transactions Journal of Vibration, Acoustics, Stress, and Reliability in Design, *110*, (3), pp. 281-287 (1988).

Childs, D. W., Nicks, C. E., Scharrer, J. K., Elrod, D. A., and Hale, R. K., , "Theory Versus Experiment for the Rotordynamic Coefficients of Annular Gas Seals: Part I - Test Facility and Apparatus," ASME Journal of Tribology, *108*, pp. 426-432 (1986).

Egli, A., "The Leakage of Steam Through Labyrinth Seals," Trans. ASME, *57*, pp. 115-122 (1935).

Elrod, D., Nelson, C., and Childs, D., "An Entrance Region Friction Factor Model Applied to Annular Seal Analysis: Theory Versus Experiment for Smooth and Honeycomb Seals," ASME Journal of Tribology, *111*, pp. 337-343 (1988).

Glassman, A. J., ed., Turbine Design and Application, NASA SP-290, *2* (1978).

Ha, T. W., "Friction Factor Data for Flat Plate Tests of Smooth and Honeycomb Surfaces," Texas A&M Turbomachinery Lab Report TL-Seal-1-89 (1989).

Liquid Rocket Engine Turbopump Rotating-Shaft Seals, NASA SP-8121 (Date?).

Nelson, C., "Analysis for Leakage and Rotordynamic Coefficients of Surface Roughened Tapered Annular Gas Seals," ASME Journal of Engineering for Gas Turbines and Power, *106*, (4), pp. 927-934 (1984).

Scharrer, J. K., "Theory Versus Experiment for the Rotordynamic Coefficients of Labyrinth Gas Seals: Part I - A Two-Control-Volume Model," ASME Transactions Journal of Vibration, Acoustics, Stress, and Reliability in Design, *110*, (3), pp. 270-280 (1988).

Schlichting, H., Boundary Layer Theory, New York, New York: McGraw-Hill, 7th ed (1979).

Wyssmann, H. R., Pham, T. C., and Jenny, R. J., "Prediction of Stiffness and Damping Coefficients for Centrifugal Compressor Labyrinth Seals," ASME Journal of Engineering for Gas Turbines and Power, *106*, pp. 920-926 (1984).